ACS Chemical Neuroscience

Research Article

pubs.acs.org/chemneuro

Early Sodium Dodecyl Sulfate Induced Collapse of α-Synuclein Correlates with Its Amyloid Formation

Sujit Basak,[†] G. V. R Krishna Prasad,[‡] Jobin Varkey,[§] and Krishnananda Chattopadhyay*[,†]

[†]Protein Folding and Dynamics Laboratory Structural Biology and Bioinformatics Division CSIR-Indian Institute of Chemical Biology (IICB) 4, Raja S.C. Mullick Road, Kolkata-700032, India

[‡]Department of Biological Sciences, Indian Institute of Science Education and Research, Sec 81, SAS Nagar, Mohali, Punjab-140306, India

[§]Centre for Converging Technologies, University of Rajasthan, Jaipur-3002004, India

Supporting Information

ABSTRACT: The aggregation of α-synuclein (A-syn) has been implicated strongly in Parkinson's disease (PD). In vitro studies established A-syn to be a member of the intrinsically disordered protein (IDP) family. This protein undergoes structural interconversion between an extended and a compact state, and this equilibrium influences the mechanism of its aggregation. A combination of fluorescence resonance energy transfer (FRET) and fluorescence correlation spectroscopy (FCS) has been used to study the membrane induced conformational reorganization and aggregation of A-syn. Different structural and conformational events, including the early collapse, the formation of the secondary structure, and aggregation have been identified and characterized using FCS and other biophysical methods. In addition, the concentrations of glycerol and urea have been varied to study the effect of solution conditions on the above conformational events. Further, we have extended this study on a number of A-syn mutants, namely, A30P, A53T, and E46K. These mutants are chosen because of their known implications in the disease pathology. The variation of solution conditions and mutational analyses suggest a strong correlation between the extent of early collapse and the onset of aggregation in PD.

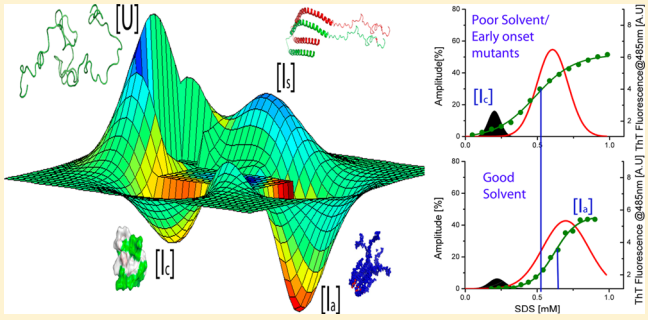

KEYWORDS: *Neurodegeneration, Parkinson's disease, intrinsically disordered protein, fluorescence resonance energy transfer, fluorescence correlation spectroscopy, single molecule fluorescence*

Protein aggregation has been implicated directly in several neurodegenerative diseases.[1] The mechanism of aggregation has been extensively studied for different proteins and polypeptides, including α-synuclein (A-syn), amyloid β, and Islet amyloid polypeptides to name a few. Aggregation of proteins may lead to loss of functions, including vesicular recycling,[2] maintenance of SNARE protein complex,[3] modulation of neural plasticity,[4] neurotransmitter release,[5] and so forth. However, the physiological functions of many of these proteins, including A-syn, are still not understood. Extensive in vitro studies place A-syn as a member of the intrinsically disordered protein (IDP)[6] family. A-syn is believed to bind to its biological partner in need for the maintenance of the biological functions.[7]

The primary structure of A-syn consists of three regions: a basic N-terminal domain, an acidic C-terminal domain, and a hydrophobic NAC region. Detailed studies involving NMR,[8] circular dichroism,[9] electron paramagnetic resonance,[10−12] fluorescence,[13,14] and other biophysical techniques[15] confirm the involvement of the basic N-terminal domain during its binding to the membrane and lipid mimic partners.[16] On interaction with the membrane, the protein forms α helical structure, with several factors such as the curvature,[17] lipid composition of the membrane,[18] the ratio of protein to lipid,[18−20] and ionic strength of the solution playing crucial roles. The presence of elongated and bent helix intermediates[21] in the presence of membrane has generated extensive interests.

A-syn, in the presence of external stress, aggregates to form amyloid fibrils, which are rich in β structure.[22] During the aggregation process, monomeric protein generates matured fibrilar structures through the formation of several oligomeric intermediates[23] encompassing many conformational states. It has been suggested that the early oligomeric intermediates, and not the matured fibrils, are toxic in the pathogenesis of Parkinson's disease (PD).[24] A number of computational[25] and experimental[26−28] studies have suggested that intrinsically disordered A-syn or its disordered state ensemble[29] (DSE) experiences structural reorganizations in the folding condition through the formation of an early collapsed state.[14,30] This

Received: July 30, 2014
Revised: October 31, 2014
Published: November 4, 2014

   dx.doi.org/10.1021/cn500168x | ACS Chem. Neurosci. 2015, 6, 239−246

event is followed by the reconsolidation of the folded state or aggregation depending upon the solution conditions. Although it is a general belief that the early collapse is hydrophobic,[27] the involvement of hydrogen bonding and backbone interaction may need to be considered. The potential energy landscape of A-syn, and arguably other IDPs, is characterized by the competition between intra- (early collapse and folding) and interchain (aggregation) interactions,[31] in which different factors including hydrophobicity, electrostatics, and solution quality play crucial roles.[32] This energy landscape is inherently complex[33] and heterogeneous requiring combined use of different biophysical techniques.[34,35]

In the present study, we have used a combination of fluorescence resonance energy transfer (FRET) and fluorescence correlation spectroscopy (FCS) to study sodium dodecyl sulfate (SDS) induced intra- (collapse) and interchain (aggregation) processes of A-syn at single molecule resolution. FCS data has been complemented by far UV circular dichroism (CD), which provides ensemble averaged information on the secondary structure. In addition, the steady state fluorescence emission of thioflavin T (THT) has been used to study the aggregation in the presence of SDS. The concentration of SDS has been maintained below 1 mM to avoid the contributions of SDS micelles. The critical micellar concentrations (cmc's) of SDS in the present experimental conditions have been determined using light scattering methods. The collapse and oligomer formation of A-syn have been investigated at different solution conditions and using three mutant proteins, namely, A53T, E46K, and A30P. These mutants have known implications to PD. Our results show that, in the case of both wild-type A-syn and the three mutants, the extent of compaction accompanied by early collapse is correlated with the onset of aggregation in different solution conditions.

RESULTS AND DISCUSSION

The FRET FCS experiment is explained in Figure 1a. A mixture of Alexa488Maleimide (Alexa488) and Alexa546Maleimide (Alexa546) coupled A-syn was used. Since the protein does not have a cysteine residue, a G132C mutation was introduced for the maleimide labeling. Neither the cysteine mutation nor the coupling by the fluorophores changed the secondary structure as determined by far UV CD measurements (Figure 1S, Supporting Information). In addition, the aggregation kinetics of G132C was found to be similar to that of the wild type (WT) protein (Figure 2S, Supporting Information). It may also be mentioned that this particular cysteine mutant was previously used in the literature.[36] FRET-FCS measurements at the donor channel would provide information about the conformation change of the protein monomer (intrachain interaction) and also on the change in size due to oligomer formation. In contrast, the data obtained at the acceptor channel would provide information about the hydrodynamics of the protein oligomers (interchain interaction between two labels).

The FRET measurements as outlined above assume that the presence of unlabeled protein does not significantly affect the aggregation kinetics of A-syn. To verify this assumption, we repeated FRET experiments using different concentrations of unlabeled and labeled A-syn proteins (Figure 3S, Supporting Information). Although the extents of FRET varied in these measurements, the trends were found similar (Figure 3S, Supporting Information).

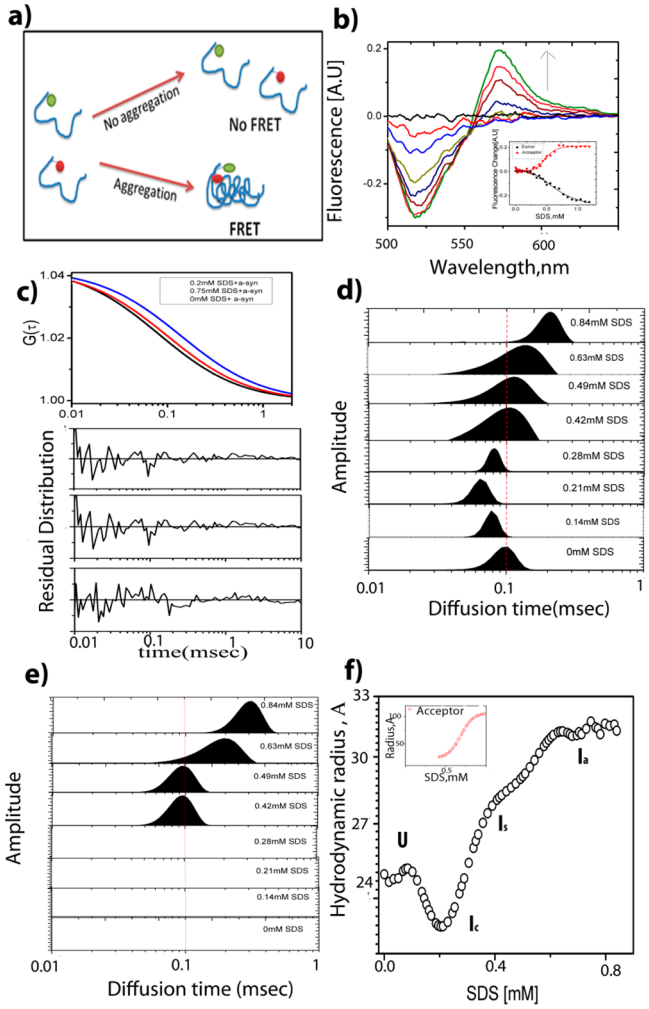

Figure 1. (a) Pictorial description of the FRET FCS experiments. (b) The fluorescence intensity at the donor emission maximum (520 nm) decreased and that at the acceptor maximum (570 nm) increased when increasing concentration of SDS was added to a mixture of Alexa488 and Alexa546 labeled A-syn; excitation wavelength is 488 nm. The inset shows the change in the intensity at the donor and acceptor channels, which complement each other. (c) Variations of the correlation functions obtained at the donor emission with the increasing concentrations of SDS. The data were fit to a model assuming the diffusion of a single component and the randomness of the residual distributions are shown at the bottom of the figure; the red, black, and blue traces correspond to 0, 0.2, and 0.75 mM SDS concentrations, respectively. SDS concentration dependence of the MEM profiles obtained at the (d) donor and (e) acceptor channels. (f) Variations of r_H with SDS concentrations at the donor channel. The data obtained at the acceptor channel are shown in the inset.

In the present study, the concentration of SDS was varied between 0 and 1 mM. Although the cmc of SDS has been reported to be 8 mM in water,[37] variation in its value has been observed in experimental solutions, notably in the presence of a protein.[15] We used light scattering measurements to determine the cmc of SDS in the absence and presence of 20 μM unlabeled A-syn (Figure 4S, Supporting Information). The present results show that cmc's of SDS both in the absence (2.5 mM) and in the presence of 20 μM A-syn (1.1 mM) are less compared to that in water (8 mM). The value of cmc in the presence of 20 μM A-syn was further substantiated by independent dynamic light scattering experiments (Figure 5S,

dx.doi.org/10.1021/cn500168x | ACS Chem. Neurosci. 2015, 6, 239−246

Supporting Information), which showed identical results. The maximum concentration of SDS used in the present study was 1 mM to minimize the contribution of SDS micelles.

In the presence of SDS concentration less that 0.4 mM, we did not observe any FRET at the emission wavelength of 570 nm (excitation wavelength of 488 nm) (Figure 1b). The FRET intensity started increasing after 0.4 mM SDS, which took place simultaneously with the decrease in the donor emission intensity (520 nm). Consequently, the steady state FRET measurements suggested the formation of oligomeric species starting at 0.4 mM SDS concentration.

The correlation functions obtained at the donor channel (Alexa488 emission) (Figure 1c) showed a decrease in the diffusion time (τ_D) in the presence of low SDS concentration (0.2 mM SDS). However, τ_D (calculated from the data obtained at the donor channel) started increasing above 0.2 mM SDS (Figure 1d). We did not obtain significant emission count below 0.4 mM to be able to calculate the correlation function at the acceptor (FRET) channel. Above 0.4 mM SDS, the values of τ_D obtained at the acceptor channel started to increase with the increase in SDS concentration, suggesting the formation of oligomeric species (Figure 1e).

Figure 1d and e shows τ_D distributions derived using the maximum entropy method (MEM) analyses of the correlation functions obtained in the donor and acceptor channels, respectively. The values of τ_D were used to calculate r_H of the protein. The values of r_H obtained from the MEM analyses at the donor channel are shown in Figure 1f (the corresponding data obtained at the acceptor channel are shown in the inset). The variation of r_H obtained at the donor channel is triphasic; a decrease in r_H at low SDS concentration (<0.2 mM), followed by a biphasic increase occurring above 0.2 mM SDS. In contrast, the MEM analyses of the correlation functions obtained at the acceptor channel showed one extended phase of increase in r_H, observed in the presence of relatively high SDS concentration (>0.4 mM). Comparing the data obtained at the donor and acceptor channels, it can be concluded that the initial decrease in r_H corresponds to an intrachain collapse (formation of I_c, Figure 1f), while the biphasic increase results in the formation of two species, I_s and I_a (Figure 1f). The comparison between the data obtained at the donor and acceptor channel clearly suggest that I_a is oligomeric. In contrast, the absence of FRET associated with I_s indicates that this intermediate may be a monomer. An independent dynamic light scattering experiment suggested a small increase in hydrodynamic diameter (3.8 Å) as a result of I_s formation (Figure 6S, Supporting Information). This change corresponds to a modest increase in the molecular weight of 8 kDa (assuming spherical shapes for all the molecules). This small change ruled out multimer formation, confirming FRET FCS data. In contrast, the increase of 8 kDa accounts for the attachment of approximately 28 molecules of SDS monomers per molecule of A-syn (assuming the molecular weight of a SDS monomer to be 0.28 kDa).

Representing the initial intrinsically disordered state of A-syn using U, the FRET FCS data can be schematically shown as follows:

Far UV CD of A-syn (in aqueous buffer and in the absence of SDS) confirmed its natively unfolded nature (Figure 6S, Supporting Information). In the presence of increasing concentration of SDS, an increase in the ellipticity at 222 nm was observed, suggesting the formation of alpha helical structure (Figure 7S, Supporting Information). An analysis using K_2D_2 (www.k2d2.ogic.ca)[38] suggested the presence of approximately 80% helical content at this condition. In addition, the presence of SDS resulted in the increase in the fluorescence emission intensity of THT, indicating the generation of amyloid-like aggregates (Figure 7S, Supporting Information). Independent transmission electron microscopy experiments (TEM; Figure 8S, Supporting Information), which were carried out with the THT active samples, supported the presence of aggregated structures. The data obtained from the far UV CD and THT fluorescence are compared in Figure 2.

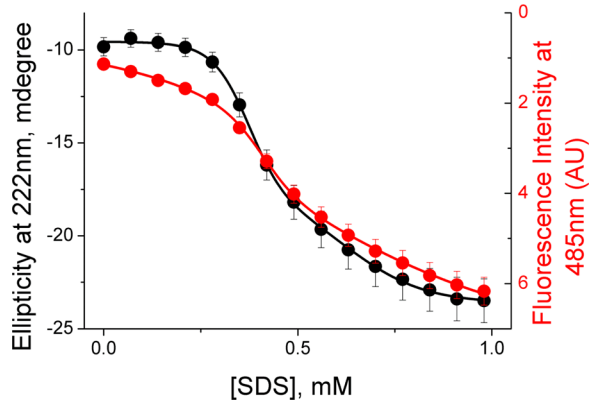

Figure 2. Variation of THT binding (red) and ellipticity at 222 nm (black) with the increase in SDS concentrations. Data were fit to a three state transition model.

Figure 2 suggests that the intermediate I_s contains significant secondary structure (about 60%), while about 24% THT fluorescence enhancement occurs in this stage. In contrast, the formation of I_a accounts for about 40% and 76% change in the far UV CD and THT fluorescence change, respectively. The midpoints of the formation of I_c, I_s, and I_a (0.15, 0.3, and 0.6 mM SDS respectively) were determined by the FCS data.

To summarize all the above results, the earliest step of the SDS induced conformational reorganizations involves a chain compaction (the formation of I_c). I_c is a compact monomer (with r_H of 22 Å) without any secondary structure. The majority of the secondary structure forms in the second step, which results in the formation of an α helical intermediate (I_s). The early formation of the collapsed structure followed by the induction of the secondary structure was observed in the salt induced refolding of two globular proteins, predominantly α helical cytochrome c[27] and the intestinal fatty acid binding proteins containing β-sheet secondary structure.[39] It is interesting that a similar pattern could be generalized in the case of an intrinsically unfolded protein, like A-syn. The formation of I_s is not accompanied by any significant FRET, suggesting I_s to be an extended monomer with r_H of 28.5 Å. The presence of extended monomeric conformation of A-syn has been reported before,[14] the nature of which is extensively debated. ESR studies indicated that the intermediate to be an extended helix with 11 Lys residues oriented perpendicular to the helix axis and 8 Glu residues in the upward direction.[10] In contrast, NMR measurements suggested a broken helix structure.[40] In this broken helix form, the protein forms two antiparallel α helices (3−37 and 45−92 residues) flanked by a ordered loop. Membrane induced conformational switching is also observed, and this switch depends on multiple factors, including the charge, chemical composition, and the curvature of the membrane.[17] The formation of I_a is accompanied by

dx.doi.org/10.1021/cn500168x | ACS Chem. Neurosci. 2015, 6, 239−246

small change in the secondary structure (about 30%). In contrast, this step accounts for a large enhancement of THT fluorescence.

The disordered to ordered transition (the molecular collapse) and its implications in protein folding have been extensively studied for both globular and intrinsically unfolded proteins.[41,42] Using cytochrome c, we showed that the interconnection between the molecular collapse and secondary structure formation depends on the nature of solvent.[27] The role of mutations in early collapse and in the aggregation has been noted in the case of the intestinal fatty acid binding proteins (IFABP).[39] It has been suggested that the incorrectly formed contacts as a part of early unfolded state reorganization needs to be broken to enable the formation of the properly folded proteins.[43]

Further, we studied the effects of different solvents and mutations using FRET FCS, far UV CD, and THT fluorescence intensity. Urea was chosen as a representative good solvent which favors backbone−solvent interaction as opposed to the backbone−backbone interaction. Indeed, FCS experiments showed diminished extents of early collapse as the concentration of urea increased (Figure 3a). As mentioned, the extent

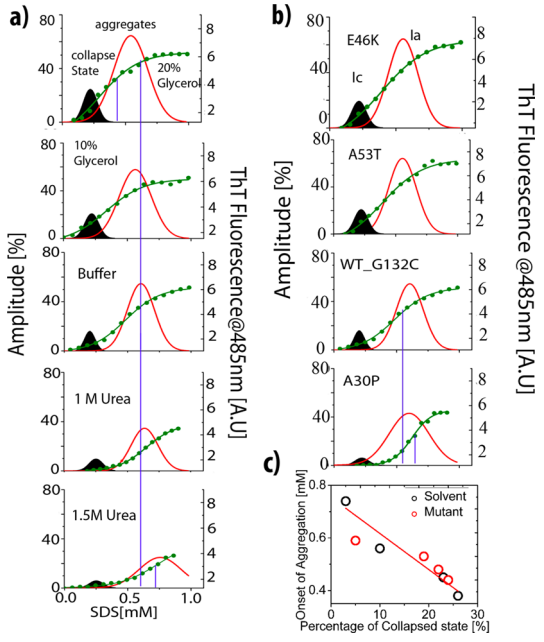

Figure 3. Variations of the extent of collapse and the onset of amyloid formation with the (a) nature of solvent and (b) nature of mutants. The black and red curves were obtained from the FCS-FRET data and refer to the I_c and I_a states, respectively. The green curves were obtained from the THT fluorescence data. The blue line represents I_a formation in normal buffer condition. The shift from this line indicates the effect of a solution condition or a mutation on A-syn aggregation. The dependence between the extent of collapse and the onset of amyloid formation is shown in (c). Black and red symbols in (c) represent the data obtained for the solvent and mutant variations, respectively.

of collapse was calculated by the difference in r_H observed by the FCS data collected at the donor channel. The measured difference in r_H was associated with the formation of I_c, the earliest event of Scheme 1, discussed above. In addition, the increase in urea concentration resulted in an increase in the onset concentration of SDS, which was measured using THT

Scheme 1. SDS Induced Conformational Reorganization and Aggregation of A-Syn

$$U \rightleftharpoons Ic \rightleftharpoons Is \rightleftharpoons Ia$$

fluorescence intensity (Figure 3a). In the second set of experiments, we used glycerol, a solution condition, which is known to favor the backbone−backbone interaction. FCS measurements showed greater extent of early collapse associated with the formation of I_c. In addition, the addition of glycerol favored amyloid formation by decreasing the onset concentration (Figure 3a). To summarize, a solvent which disfavors backbone−backbone interaction, seems to delay amyloid formation. Next, we tested three mutant proteins, namely, A30P, E46K, and A53T, to find out if a similar correlation existed. These mutations are known to have strong implications in PD.

The extent of early collapse is significantly higher in the case of E46K and A53T mutants compared to that observed in WT and A30P (Figure 3b). In contrast, measurement of THT fluorescence intensity showed that the propensity to form amyloid was the greatest for A53T and E46K mutants (Figure 3b). A30P was found to have the most delayed onset of amyloid formation (Figure 3b).

Figure 3c plots the correlation between the onsets of amyloid formation and the extent of early collapse for the WT protein in the presence of different concentrations of urea and glycerol. These two parameters showed excellent correlation, with the correlation coefficient being 0.9. The extent of collapse and the onset of amyloid formation data obtained with the three mutants are also shown in the same figure using the open red circles. It is interesting to note that the mutants' data also fall nicely on the correlation line.

The interaction between A-syn and membrane (or membrane mimic, like SDS) has been studied extensively. Single molecule fluorescence spectroscopy and other biophysical techniques have been used to study the binding and conformational switching in the presence of SDS.[14,15,26,44] These studies have found the presence of multiple intermediates of A-syn, which have been induced and stabilized at different concentrations of SDS.[44] The present FCS measurements, which directly determine hydrodynamic radius, agree well with the initial increase in the FRET efficiency observed by Ferreon et al. in their single molecule FRET measurements.[14] The extent of secondary structure formation is found to be dependent on multiple factors, including the nature of membrane mimics, protein membrane ratio, and the membrane curvature.[17] Ahmad et al. have shown the predominance of fibrillogenic aggregates at low concentration of SDS (less than 1 mM), a conclusion supported by the present data. In contrast, the addition of SDS micelles (>1 mM) results in the inhibition of fibrillation.[45] Giehm et al. have used a number of spectroscopic and biophysical techniques to suggest an alternative fibrillation pathway populated in the presence of SDS.[15] This pathway differs significantly from the classical aggregation of A-syn, which takes place in the absence of SDS.[15]

Although the implication of these mutants to PD has been noted, any mechanistic interpretation of their roles is unknown. The present results correlate the mutant properties nicely with a physical interpretation obtained from the solvent data, clearly suggesting a direct contribution of the backbone−backbone interactions. An explanation of the present data may consider

dx.doi.org/10.1021/cn500168x | ACS Chem. Neurosci. 2015, 6, 239−246

the binding between A-syn and membrane (or membrane mimics, like SDS in this case) into account. The presence of low concentration of SDS (like what is used in the present study) can confine the protein in a small one- or two-dimensional space, resulting in high local concentration of the protein.[46] In an another model, small micelles of four to seven SDS molecules or small tubules sharing a protein chain have been proposed in the studied range of protein concentration, resulting in amyloid formation. It is interesting to note that these oligomers or short micelles can form in SDS concentrations less than its cmc.[15] In this explanation, the facilitation of micellization and/or the binding between the protein and SDS micelles plays crucial roles on the onset (and also on the extent) of amyloidosis. This explanation holds for the A53T and E46K proteins, which have higher propensities for amyloid formation. These proteins have higher membrane affinities compared to A30P. This is known that A30P is less likely to form amyloid. However, the present results obtained with urea and glycerol does not completely agree with this explanation. This is because both urea and glycerol are known to inhibit the formation of SDS micelles,[47] although they behave differently to the amyloid formation propensity as shown here.

A second possibility may come from the interplay between the early intrachain reorganization of the protein and the subsequent aggregation. The correlation between the early conformational change and aggregation has been a matter of extensive debate. The presence of extended conformation has been noted using tryptophan-cysteine contact quenching by measuring the kinetics of loop closure of polyglutamine peptides.[48] In contrast, the chain length of polyglutamine peptide has been shown to play a direct role in the peptide collapse.[49] The age of onset of Huntington's diseases is found to have inverse correlation with the length of polyglutamine domain.[50] Along this line, a connection between polyglutamine length and the increase in aggregation has been observed, which supports the present data. Both computational and experimental studies[27,31]suggest that early intramolecular collapse events leading to incorrect contact formations (or misfolding) needs to be corrected by subsequent slow steps, else these could lead to aggregation.[51] It has been demonstrated that the aggregation kinetics of A-syn, which is a slow process, can be controlled kinetically by chain reorganization at the early microsecond.[35]

The spectroscopic understanding of protein amyloidosis is complicated because the energy landscape of misfolding is heterogeneous. Another difficulty arises from the slowness of protein aggregation. The present data as well as other recent results, however, show strong correlation between the early (which may be hidden in the initial phase) and the late stages of amyloid formation. In addition, the early oligomers are believed to be more toxic than the matured fibrils.[52] Taken together, detailed understanding of the early events of protein aggregation may be essential not only for the molecular level understanding of this process, but also for the development of a suitable pharmaceutical strategy to counter the aggregation related threats.

METHODS

Materials and Methods. For the purification of A-syn and its mutants, we purchased isopropyl β-D-galactopyranoside (IPTG) and Tris salt from Biotecx Laboratories (Houston, TX) and J.T. Baker (Center Valley, PA), respectively. Phenylmethanesulfonylfluoride (PMSF), ammonium sulfate, and sodium chloride were obtained from Sigma-Aldrich (St. Louis, MO). For high performance liquid chromatography (HPLC), we used two columns of Waters (Milford, MA). Urea and NaH_2PO_4 were obtained from Sigma-Aldrich (St. Louis, MO). Glycerol and sodium dodecyl sulfate (SDS) were purchased from Merck (Whitehouse Station, NJ) and USB (Cleveland, OH), respectively.

Protein Purification of A-Syn. Recombinant human A-syn and its mutants were expressed in *Escherichia coli* BL21 (DE3) strain transformed with pRK172 α-synuclein WT/mutant plasmid. The expression was induced using 1 M IPTG at an OD of 0.5−0.6. The cultures were incubated at 37 °C with shaking at 175 rpm for 4 h after addition of IPTG. Cells were then harvested by centrifugation. The cell pellets were then resuspended in sonication buffer (10 mM Tris, pH = 7.4) and lysed by sonication using short but continuous pulses at 12 Hz for 1 min. This step was repeated 14 times to lyse all the cells. The lysate was centrifuged at 14 000 rpm for 45 min at 4 °C to remove cell debris. Just before the sonication, 1 mM PMSF cocktail was added. The lysis suspension was brought to 30% saturation with ammonium sulfate and the pellet was discarded. It was followed by 50% saturation with ammonium sulfate. The solution was then centrifuged at 35 000 rpm for 1 h at 4 °C. The resultant pellet was dissolved in 10 mM Tris buffer, pH 7.4 and dialyzed overnight against same buffer. After dialysis, the protein sample was filtered using 30 kDa centricon filter. The crude protein was then injected into a DEAE anion exchange column equilibrated with 10 mM Tris (pH = 7.4) and eluted using a NaCl gradient. A-syn was found to elute at about 300 mM NaCl. Fractions containing A-syn (analyzed by coomassie-stained SDS-PAGE) were concentrated and further purified using a Sephadex gel filtration column. Fractions containing A-syn were combined and lyophilized. The protein was determined to be about 95% pure by SDS-PAGE. For the experiments with A53T, E46K, and A30P proteins, corresponding double mutants with additional G132C mutations were used with each case.

For the sample preparations of all experiments, lyophilized protein was dissolved in sodium phosphate buffer (pH 7.4) and filtered using 0.22 μm low protein binding membranes (Millex-GP). This step is essential because the presence of small amount of oligomers can act as seeds for further aggregation.

FRET-FCS Setup. FRET-FCS experiments were carried out in the presence of different SDS concentration in 20 mM NaH_2PO_4 pH 7.4. These measurements were performed using a Confocor 3 LSM system. Excitation was achieved by focusing the 488 nm line of an argon laser into the sample solution, 50 μm above the glass coverslip surface, using a water immersion objective (1.2 NA, 40×; Carl Zeiss). The fluorescence emission was collected using the same objective, separated from the excitation light using a dichroic filter. The emission line was spatially filtered using a 70 μm pinhole, which was then split into donor and acceptor components using a mirror (NT 50/50 IR). The donor and acceptor signals were further filtered using a BP 505−540 IR band pass filter and a BP 560−610 IR band pass filter, respectively. The emission was detected using two avalanche photodiode (APD) photon counting modules. Photon counts were recorded using a photon counting card interfaced with a computer. Microscope correction collar and height were adjusted manually to correct for refractive index mismatch between the immersion solution and experimental environment. All protein data was normalized using the τ_D value obtained with the free dye (alexa488 maleimide) measured under identical condition.

Fluorescence intensity emitted from the small confocal volume is collected as a function of time. The recorded fluorescence intensity fluctuates as the fluorescently labeled molecules diffuse in and out of the confocal volume. The fluctuations of fluorescence intensity, which consist of information on the average number of molecules, the resident time of the molecule, and other photophysical properties, can be analyzed using the autocorrelation function. The normalized form of the autocorrelation function of intensity $I(t)$ at time t is represented by

dx.doi.org/10.1021/cn500168x | ACS Chem. Neurosci. 2015, 6, 239−246

$$G(\tau) = \frac{\langle \delta I(t+\tau)\delta I(t)\rangle}{\langle I(t)\rangle^2} \quad (1)$$

In this expression, $\langle I(t)\rangle$ is the average of the fluorescence signal over time and $\delta I(t)$ is the signal fluctuation at time t minus the average: $\langle \delta I(t)\rangle = I(t) - \langle I(t)\rangle$.

For a simple system of the diffusion of a one component, the autocorrelation function can be defined by the following equation:

$$G(\tau) = 1 + \frac{1}{N}\frac{1}{\left(1+\frac{\tau}{\tau_D}\right)}\frac{1}{\left(1+S^2\frac{\tau}{\tau_D}\right)^{1/2}} \quad (2)$$

where N is the number of the molecules present in the confocal volume and can be calculated from the $N = 1/G(0)$ relationship. S is the structural parameter, which is defined by the ratio of beam radius and height. For a FCS experiment, the characteristic diffusion time (τ_D) is related to the diffusion coefficient (D) by the following equation:

$$\tau_D = \frac{\omega^2}{4D} \quad (3)$$

where ω defines the size of the observation volume. The value of hydrodynamic radius (r_H) can be obtained from D using the Stokes–Einstein formalism (eq 4).

$$D = \frac{kT}{6\pi\eta r_H} \quad (4)$$

In our experiments, typically 100 nM Alexa488 labeled A-syn along with 20 μM unlabeled protein was used.

Maximum Entropy Method (MEM) Analysis of the Correlation Functions. FCS data was analyzed further using MEM, which determines the distribution of α_i of a heterogeneous system on the basis of maximum entropy S and minimum χ^2. S is defined by

$$S = -\sum p_i \ln p_i \quad (5)$$

where $p_i = \alpha_i/\Sigma\alpha_i$.[53]

Thioflavin T (ThT) Binding fluorescence Assay. A volume of 3 mL of 20 μM A-syn with 20 μM of ThT in 20 mM sodium phosphate buffer pH 7.4 was titrated with 0–1 mM SDS in a quartz cuvette of 1 cm path length. Slits for this experiment were at 2 nm for excitation and emission each, and integration time was 1 s. While adding SDS, steady state fluorescence was monitored using excitation at 450 nm and emission at 485 nm with proper mixing. Fluorescence measurements were carried out using a PTI fluorimeter. After sample preparation, samples were kept in 37 °C incubator for 2 h with constant stirring at 200 rpm.

Circular Dichroism. A volume of 800 μL of 20 μM unlabeled A-syn in 20 mM NaH_2PO_4 buffer at pH 7.4 was kept at different SDS concentrations for 2 h in constant agitation, and the secondary structure change of each sample was monitored using a JASCO J 720 CD instrument. Other parameters included scan speed at 100 nm/min, integration time of 1 s, and number of scans of 5. CD measurements were carried out between 200 and 250 nm using the permissible HT voltage to obtain optimum signal-to-noise ratio. A traditional CD cuvette of 0.1 cm path length was used for the far UV CD measurements.

Transmission Electron Microscopy. A total of 5 μL of A-syn of 20 mM concentration in 20 mM sodium phosphate buffer pH 7.4 with various surfactant concentrations was transferred to a 400-mesh carbon-coated glow-discharged grid.

After 30 s of incubation, grids were washed in two drops of doubly distilled water, stained with 2% uranyl acetate solution, and blotted dry on filter paper. Then samples were kept for overnight in a desiccator to dry the samples. Samples were viewed on a transmission electron microscope.

Static and Dynamic Light Scattering. Static light scattering (SLS) experiment was carried out using a PTI fluorimeter with the excitation and emission wavelengths at 350 nm. A xenon lamp was used in the SLS experiment. The scan speed was 30 points/s, and excitation and emission slits were kept at 2 nm each. The signals were collected in the detector placed at 90°.

The Malvern Zetasizer Nano ZS DLS system (Malvern Instruments Ltd., UK) was used to perform all dynamic light scattering (DLS) measurements. The DLS system is equipped with a 633 nm He–Ne laser and an avalanche photodiode detector configured to collect backscattered light at 173°. The sample was maintained at 25 °C and allowed to equilibrate for 120 s prior to analysis. Each size measurement was determined from 10 runs, 10 s each. All DLS data were collected and analyzed using Malvern Zetasizer 6.12 software. All reported mean particle hydrodynamic radii (R_H) were calculated from intensity based particle size distributions.

■ ASSOCIATED CONTENT

Supporting Information

Additional figures as described in the text. This material is available free of charge via the Internet at http://pubs.acs.org.

■ AUTHOR INFORMATION

Corresponding Author

*E-mail: krish@iicb.res.in.

Author Contributions

KC wrote the paper. SB, GVRKP and JV prepared the initial protein samples, SB carried out the experiments, SB and KC analyzed the data. All authors reviewed the paper.

Funding

This study has been funded by CSIR network Project Grant MIND.

Notes

The authors declare no competing financial interest.

■ ACKNOWLEDGMENTS

The authors thank Prof. Sudipta Maiti for the MEM FCS software. KC thanks the director, CSIR-IICB for his help and encouragement. JV is supported by DBT Ramalingaswami fellowship. The authors thank Dr. Ralf Langen of the University of Southern California for his help.

■ REFERENCES

(1) Goedert, M. (2001) Alpha-synuclein and neurodegenerative diseases. *Nat. Rev. Neurosci. 2* (7), 492–501.

(2) Sancenon, V., Lee, S. A., Patrick, C., Griffith, J., Paulino, A., Outeiro, T. F., Reggiori, F., Masliah, E., and Muchowski, P. J. (2012) Suppression of alpha-synuclein toxicity and vesicle trafficking defects by phosphorylation at S129 in yeast depends on genetic context. *Hum. Mol. Genet. 21* (11), 2432–2449.

(3) Chandra, S., Gallardo, G., Fernandez-Chacon, R., Schluter, O. M., and Sudhof, T. C. (2005) Alpha-synuclein cooperates with CSPalpha in preventing neurodegeneration. *Cell 123* (3), 383–396.

(4) Sidhu, A., Wersinger, C., and Vernier, P. (2004) Does alpha-synuclein modulate dopaminergic synaptic content and tone at the synapse? *FASEB J. 18* (6), 637–647.

(5) Bendor, J. T., Logan, T. P., and Edwards, R. H. (2013) The function of alpha-synuclein. *Neuron 79* (6), 1044–1066.

(6) Dunker, A. K., Lawson, J. D., Brown, C. J., Williams, R. M., Romero, P., Oh, J. S., Oldfield, C. J., Campen, A. M., Ratliff, C. M., Hipps, K. W., Ausio, J., Nissen, M. S., Reeves, R., Kang, C., Kissinger, C. R., Bailey, R. W., Griswold, M. D., Chiu, W., Garner, E. C., and Obradovic, Z. (2001) Intrinsically disordered protein. *J. Mol. Graphics Modell. 19* (1), 26–59.

(7) Lee, F. J., Liu, F., Pristupa, Z. B., and Niznik, H. B. (2001) Direct binding and functional coupling of alpha-synuclein to the dopamine transporters accelerate dopamine-induced apoptosis. *FASEB J. 15* (6), 916–926.

(8) Wang, G. F., Li, C., and Pielak, G. J. (2010) 19F NMR studies of alpha-synuclein-membrane interactions. *Protein Sci. 19* (9), 1686−1691.
(9) Anderson, V. L., Ramlall, T. F., Rospigliosi, C. C., Webb, W. W., and Eliezer, D. (2010) Identification of a helical intermediate in trifluoroethanol-induced alpha-synuclein aggregation. *Proc. Natl. Acad. Sci. U. S. A. 107* (44), 18850−18855.
(10) Jao, C. C., Hegde, B. G., Chen, J., Haworth, I. S., and Langen, R. (2008) Structure of membrane-bound alpha-synuclein from site-directed spin labeling and computational refinement. *Proc. Natl. Acad. Sci. U. S. A. 105* (50), 19666−19671.
(11) Drescher, M., Huber, M., and Subramaniam, V. (2012) Hunting the chameleon: Structural conformations of the intrinsically disordered protein alpha-synuclein. *ChemBioChem 13* (6), 761−768.
(12) Drescher, M., van Rooijen, B. D., Veldhuis, G., Subramaniam, V., and Huber, M. (2010) A stable lipid-induced aggregate of alpha-synuclein. *J. Am. Chem. Soc. 132* (12), 4080−4082.
(13) Veldhuis, G., Segers-Nolten, I., Ferlemann, E., and Subramaniam, V. (2009) Single-molecule FRET reveals structural heterogeneity of SDS-bound alpha-synuclein. *ChemBioChem 10* (3), 436−439.
(14) Ferreon, A. C., Gambin, Y., Lemke, E. A., and Deniz, A. A. (2009) Interplay of alpha-synuclein binding and conformational switching probed by single-molecule fluorescence. *Proc. Natl. Acad. Sci. U. S. A. 106* (14), 5645−5650.
(15) Giehm, L., Oliveira, C. L., Christiansen, G., Pedersen, J. S., and Otzen, D. E. (2010) SDS-induced fibrillation of alpha-synuclein: An alternative fibrillation pathway. *J. Mol. Biol. 401* (1), 115−33.
(16) Eliezer, D. (2009) Biophysical characterization of intrinsically disordered proteins. *Curr. Opin. Struct. Biol. 19* (1), 23−30.
(17) Middleton, E. R., and Rhoades, E. (2010) Effects of curvature and composition on alpha-synuclein binding to lipid vesicles. *Biophys. J. 99* (7), 2279−2288.
(18) Shvadchak, V. V., Yushchenko, D. A., Pievo, R., and Jovin, T. M. (2011) The mode of alpha-synuclein binding to membranes depends on lipid composition and lipid to protein ratio. *FEBS Lett. 585* (22), 3513−3519.
(19) Varkey, J., Isas, J. M., Mizuno, N., Jensen, M. B., Bhatia, V. K., Jao, C. C., Petrlova, J., Voss, J. C., Stamou, D. G., Steven, A. C., and Langen, R. (2010) Membrane curvature induction and tubulation are common features of synucleins and apolipoproteins. *J. Biol. Chem. 285* (42), 32486−32493.
(20) Varkey, J., Mizuno, N., Hegde, B. G., Cheng, N., Steven, A. C., and Langen, R. (2013) alpha-Synuclein oligomers with broken helical conformation form lipoprotein nanoparticles. *J. Biol. Chem. 288* (24), 17620−17630.
(21) Lokappa, S. B., and Ulmer, T. S. (2011) Alpha-synuclein populates both elongated and broken helix states on small unilamellar vesicles. *J. Biol. Chem. 286* (24), 21450−21457.
(22) Vilar, M., Chou, H. T., Luhrs, T., Maji, S. K., Riek-Loher, D., Verel, R., Manning, G., Stahlberg, H., and Riek, R. (2008) The fold of alpha-synuclein fibrils. *Proc. Natl. Acad. Sci. U. S. A. 105* (25), 8637−8642.
(23) Sandal, M., Valle, F., Tessari, I., Mammi, S., Bergantino, E., Musiani, F., Brucale, M., Bubacco, L., and Samori, B. (2008) Conformational equilibria in monomeric alpha-synuclein at the single-molecule level. *PLoS Biol. 6* (1), e6.
(24) Wu, J. W., Breydo, L., Isas, J. M., Lee, J., Kuznetsov, Y. G., Langen, R., and Glabe, C. (2010) Fibrillar oligomers nucleate the oligomerization of monomeric amyloid beta but do not seed fibril formation. *J. Biol. Chem. 285* (9), 6071−6079.
(25) Straub, J. E., and Thirumalai, D. (2011) Toward a molecular theory of early and late events in monomer to amyloid fibril formation. *Annu. Rev. Phys. Chem. 62*, 437−463.
(26) Ferreon, A. C., Moran, C. R., Ferreon, J. C., and Deniz, A. A. (2010) Alteration of the alpha-synuclein folding landscape by a mutation related to Parkinson's disease. *Angew. Chem., Int. Ed. Engl. 49* (20), 3469−72.
(27) Haldar, S., and Chattopadhyay, K. (2012) Interconnection of salt-induced hydrophobic compaction and secondary structure formation depends on solution conditions: Revisiting early events of protein folding at single molecule resolution. *J. Biol. Chem. 287* (14), 11546−11555.
(28) Hillger, F., Hanni, D., Nettels, D., Geister, S., Grandin, M., Textor, M., and Schuler, B. (2008) Probing protein-chaperone interactions with single-molecule fluorescence spectroscopy. *Angew. Chem., Int. Ed. Engl. 47* (33), 6184−6188.
(29) Bowler, B. E. (2012) Residual structure in unfolded proteins. *Curr. Opin Struct Biol. 22* (1), 4−13.
(30) Morar, A. S., Olteanu, A., Young, G. B., and Pielak, G. J. (2001) Solvent-induced collapse of alpha-synuclein and acid-denatured cytochrome c. *Protein Sci. 10* (11), 2195−2199.
(31) Routledge, K. E., Tartaglia, G. G., Platt, G. W., Vendruscolo, M., and Radford, S. E. (2009) Competition between intramolecular and intermolecular interactions in an amyloid-forming protein. *J. Mol. Biol. 389* (4), 776−786.
(32) Fitzpatrick, A. W., Knowles, T. P., Waudby, C. A., Vendruscolo, M., and Dobson, C. M. (2011) Inversion of the balance between hydrophobic and hydrogen bonding interactions in protein folding and aggregation. *PLoS Comput. Biol. 7* (10), e1002169.
(33) Lapidus, L. J. (2013) Exploring the top of the protein folding funnel by experiment. *Curr. Opin. Struct. Biol. 23* (1), 30−35.
(34) Buell, A. K., Dhulesia, A., White, D. A., Knowles, T. P., Dobson, C. M., and Welland, M. E. (2012) Detailed analysis of the energy barriers for amyloid fibril growth. *Angew. Chem., Int. Ed. Engl. 51* (21), 5247−5251.
(35) Ahmad, B., Chen, Y., and Lapidus, L. J. (2012) Aggregation of alpha-synuclein is kinetically controlled by intramolecular diffusion. *Proc. Natl. Acad. Sci. U. S. A. 109* (7), 2336−2341.
(36) Wu, K. P., Kim, S., Fela, D. A., and Baum, J. (2008) Characterization of conformational and dynamic properties of natively unfolded human and mouse alpha-synuclein ensembles by NMR: Implication for aggregation. *J. Mol. Biol. 378* (5), 1104−1115.
(37) Paula, S., Sues, W., Tuchtenhagen, J., and Blume, A. (1995) Thermodynamics of Micelle Formation as a Function of Temperature: A High Sensitivity Titration Calorimetry Study. *J. Phys. Chem. 99* (30), 11742−11751.
(38) Perez-Iratxeta, C., and Andrade-Navarro, M. A. (2008) K2D2: Estimation of protein secondary structure from circular dichroism spectra. *BMC Struct. Biol. 8*, 25.
(39) Sarkar, S., and Chattopadhyay, K. (2014) Studies of early events of folding of a predominately beta-sheet protein using fluorescence correlation spectroscopy and other biophysical methods. *Biochemistry 53* (9), 1393−1402.
(40) Ulmer, T. S., Bax, A., Cole, N. B., and Nussbaum, R. L. (2005) Structure and dynamics of micelle-bound human alpha-synuclein. *J. Biol. Chem. 280* (10), 9595−9603.
(41) Muller-Spath, S., Soranno, A., Hirschfeld, V., Hofmann, H., Ruegger, S., Reymond, L., Nettels, D., and Schuler, B. (2010) Charge interactions can dominate the dimensions of intrinsically disordered proteins. *Proc. Natl. Acad. Sci. U. S. A. 107* (33), 14609−14614.
(42) Haran, G. (2012) How, when and why proteins collapse: The relation to folding. *Curr. Opin. Struct. Biol. 22* (1), 14−20.
(43) Horwich, A. (2002) Protein aggregation in disease: A role for folding intermediates forming specific multimeric interactions. *J. Clin. Invest. 110* (9), 1221−1232.
(44) Ferreon, A. C., and Deniz, A. A. (2007) Alpha-synuclein multistate folding thermodynamics: Implications for protein misfolding and aggregation. *Biochemistry 46* (15), 4499−4509.
(45) Ahmad, M. F., Ramakrishna, T., Raman, B., and Rao, Ch. M. (2006) Fibrillogenic and non-fibrillogenic ensembles of SDS-bound human alpha-synuclein. *J. Mol. Biol. 364* (5), 1061−1072.
(46) Dikiy, I., and Eliezer, D. (2012) Folding and misfolding of alpha-synuclein on membranes. *Biochim. Biophys. Acta 1818* (4), 1013−1018.
(47) Haldar, S., and Chattopadhyay, K. (2011) Effects of arginine and other solution additives on the self-association of different surfactants:

An investigation at single-molecule resolution. *Langmuir 27* (10), 5842−5849.
(48) Singh, V. R., and Lapidus, L. J. (2008) The intrinsic stiffness of polyglutamine peptides. *J. Phys. Chem. B 112* (42), 13172−13176.
(49) Walters, R. H., and Murphy, R. M. (2009) Examining polyglutamine peptide length: A connection between collapsed conformations and increased aggregation. *J. Mol. Biol. 393* (4), 978−992.
(50) Gusella, J. F., and MacDonald, M. E. (2000) Molecular genetics: Unmasking polyglutamine triggers in neurodegenerative disease. *Nat. Rev. Neurosci 1* (2), 109−115.
(51) Young, J. C., Agashe, V. R., Siegers, K., and Hartl, F. U. (2004) Pathways of chaperone-mediated protein folding in the cytosol. *Nat. Rev. Mol. Cell Biol. 5* (10), 781−791.
(52) Auluck, P. K., Caraveo, G., and Lindquist, S. (2010) alpha-Synuclein: Membrane interactions and toxicity in Parkinson's disease. *Annu. Rev. Cell Dev. Biol. 26*, 211−233.
(53) Sengupta, P., Garai, K., Balaji, J., Periasamy, N., and Maiti, S. (2003) Measuring size distribution in highly heterogeneous systems with fluorescence correlation spectroscopy. *Biophys. J. 84* (3), 1977−1984.